J. Phys.: Condens. Matter **20** (2008) 315001 (5pp) doi:10.1088/0953-8984/20/31/315001

Calculation of electronic stopping power along glancing swift heavy ion tracks in perovskites using *ab initio* electron density data

O Osmani[1], A Duvenbeck[1], E Akcöltekin[1], R Meyer[1], H Lebius[2] and M Schleberger[1]

[1] Department of Physics, University of Duisburg-Essen, D-47048 Duisburg, Germany
[2] CIMAP, blvd Henri Becquerel, 14070 Caen, France

E-mail: marika.schleberger@uni-due.de

Received 22 January 2008, in final form 3 June 2008
Published 26 June 2008
Online at stacks.iop.org/JPhysCM/20/315001

Abstract

In recent experiments the irradiation of insulators of perovskite type with swift ($E \sim 100$ MeV) heavy ions under glancing incidence has been shown to provide a unique means to generate periodically arranged nanodots at the surface. The physical origin of these patterns has been suggested as stemming from a highly anisotropic electron density distribution within the bulk. In order to show the relevance of the electron density distribution of the target we present a model calculation for the system $Xe^{23+} \rightarrow SrTiO_3$ that is known to produce the aforementioned surface modifications. On the basis of the Lindhard model of electronic stopping, we employ highly-resolved *ab initio* electron density data to describe the conversion of kinetic energy into excitation energy along the ion track. The primary particle dynamics are obtained via integration of the Newtonian equations of motion that are governed by a space- and time-dependent frictional force originating from Lindhard stopping. The analysis of the local electronic stopping power along the ion track reveals a pronounced periodic structure. The periodicity length varies strongly with the particular choice of the polar angle of incidence and is directly correlated to the experimentally observed formation of periodic nanodots at insulator surfaces.

(Some figures in this article are in colour only in the electronic version)

1. Introduction

The irradiation of a solid surface with a ∼100 MeV ion beam leads to the formation of cylindrical tracks within the target material (see e.g. [1–3]). This phenomenon can be explained in terms of kinetic excitation of electrons along the path of the penetrating ion. These electronic excitations are directly connected with structural changes within the damage zone which may also extend to the very surface, for instance, manifesting themselves in the formation of nanodots.

In the case of normal incidence of the ion beam the nanodots are statistically distributed over the entire irradiated area [4–7] due to the random distribution of the ion impact sites. In recent experiments [8, 9], the irradiation of perovskite crystals (ABO_3) under *glancing incidence* has been shown to provide a unique means to generate chain-like, periodic nanodots at the surface, the extension of which varies in the range from a few hundred nanometres up to some microns depending on the particular angle of incidence. This finding has been ascribed to the specific anisotropic electron density of the perovskite structure. The nanodots can be imaged by atomic force microscopy [10], for instance, and may be regarded as a fingerprint of the electron density projected onto the surface.

Although the detailed microscopic mechanisms of this kind of defect formation are not entirely understood, the anisotropy of the electron density inducing a discontinuous kinetic energy dissipation of the ion appears to play a key role.

For many practical purposes the energy loss per track length can be calculated using SRIM [11, 12] or equivalent standard codes. However, these codes are not capable of accounting for the detailed electronic structure. In addition, these codes do not provide any space-resolved information on energy losses inside the crystal, which are supposed to be essential in our case.

Therefore this paper aims at a detailed investigation of the spatial electronic energy loss under ∼100 MeV glancing incidence irradiation for the exemplary model system $Xe^{23+} \rightarrow SrTiO_3$, which has been shown to produce the aforementioned periodic nanopatterns. We combine *ab initio* electron density computations with trajectory calculations in order to study the electronic stopping dynamics along the ion track for different polar and azimuthal angles of incidence.

2. Model

For the irradiation of $SrTiO_3(100)$ with Xe^{23+} ions of ∼100 MeV of kinetic energy electronic stopping dominates over nuclear stopping by two orders of magnitude. In this energy regime electronic stopping occurs via direct inelastic projectile-electron collisions and is often treated in terms of the Lindhard model [13] yielding an electronic stopping cross section $S_e = \beta v_p$ with a material parameter β depending on the specific target–projectile combination and v_p denoting the projectile velocity. For a target containing different elements i with individual $\beta^{(i)}$'s the effective electronic stopping cross section $S_{e,eff}$ is given by

$$S_{e,eff} = \beta_{eff} v_p = \sum_i w^{(i)} \beta^{(i)} v_p \qquad (1)$$

with relative weight factors $w^{(i)}$ mirroring the stoichiometry of the target. The electronic energy loss per track length (stopping power) of the projectile along its path through the solid then reads

$$\left.\frac{dE}{dx}\right|_e = N_e(\vec{r}_p(t)) \cdot \beta_{eff} \cdot |\dot{\vec{r}}_p(t)|, \qquad (2)$$

where $N_e(\vec{r}_p(t))$ denotes the electron density of the target at the time-dependent position $\vec{r}_p(t)$ of the penetrating ion. It should be mentioned that for the system studied here the initial charge of $q = 23$ is close to the equilibrium charge state during the passage of the ion through the target [14, 15].

The electron density $N_e(\vec{r})$ constituting the *first* essential input parameter in equation (2) is calculated for one unit cell of the perovskite using the ABINIT package [16] with pseudopotentials from the Fritz–Haber-Institut [17]. Employing a cutoff energy of 96 Hartree with a sampling of 512 k-points on a cubic grid, the calculations have been carried out within the GGA approximation using the PBE functional [18]. The lattice constant of $SrTiO_3$ has been determined as 3.905 Å by minimization of the energy. It should be noted that *ab initio* calculations using pseudopotentials only give the electron density of the valence electrons. The core electrons, however, are strongly localized around the nuclei which limits their influence to a very small fraction of the volume. In the energy range we are considering here, the projectile comes close to the nuclei only very rarely. Therefore consideration of the core electrons would lead to only minor quantitative changes of our result and no qualitative changes at all.

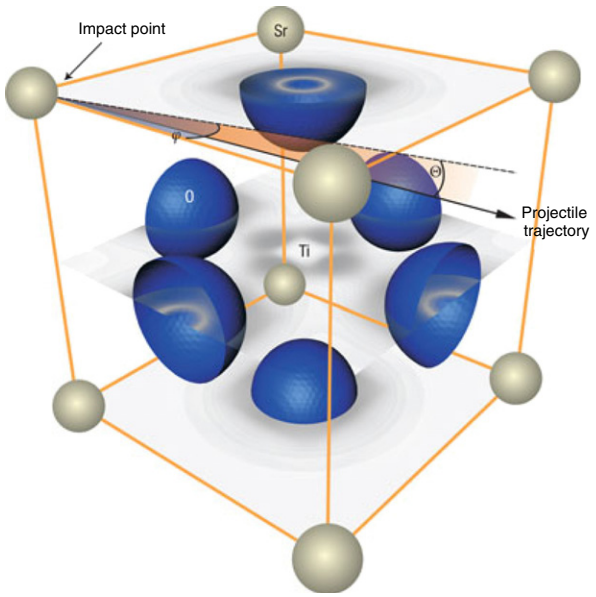

Figure 1. (Figure and caption reprinted with permission from [8].) DFT calculation of the electron density of $SrTiO_3$: the grey shading represents electron density. Atom positions (apart from the central titanium atom) are also visualized. The arrow indicates a possible projectile trajectory defined by the azimuthal angle φ as well as the incidence angle Θ.

The electron density $N_e(\vec{r})$ resulting from this *ab initio* computation is shown in figure 1. The majority of the electrons are localized around the oxygen atoms. Moreover, the electron density in the TiO_2 plane clearly exceeds the one observed in the SrO plane. Thus, it becomes directly obvious that $N_e(\vec{r})$ varies on a sub-Ångström scale and hence should not be treated as a homogeneous electron gas.

The *second* parameter to be inserted in equation (2) is the trajectory $\vec{r}_p(t)$ and its first time derivative. The trajectory is calculated by numerical integration of the Newtonian equations of motion for the projectile. In view of the fact that energy dissipation is governed by electronic stopping, in a first-order approximation no interatomic potentials have to be incorporated into the equations of motion. Thus, the only interaction between the primary ion and the target is an effective frictional force according to equation (2) that originates from Lindhard stopping. During the time integration of the ion track the energy loss per numerical time step is output for further analysis.

3. Results

The computational procedure as outlined in the previous section has been performed for the irradiation of $SrTiO_3$ with Xe^{23+} ions in the energy range from (10–100) MeV. For each bombarding energy the azimuthal angle of impact has been varied. The crystal symmetry of the target allows the azimuthal variation to be limited to the range 0° to 45°.

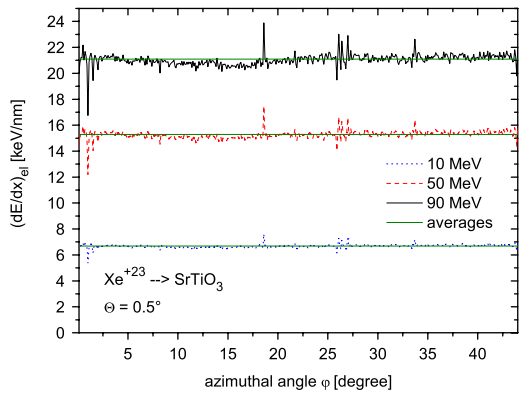

Figure 2. Average electronic stopping power $(\mathrm{d}E/\mathrm{d}x)_{\mathrm{el}}$ for different irradiation energies (10, 50, 90 MeV) and a polar angle of 0.5°. The step width $\Delta\varphi$ has been set to 0.1°.

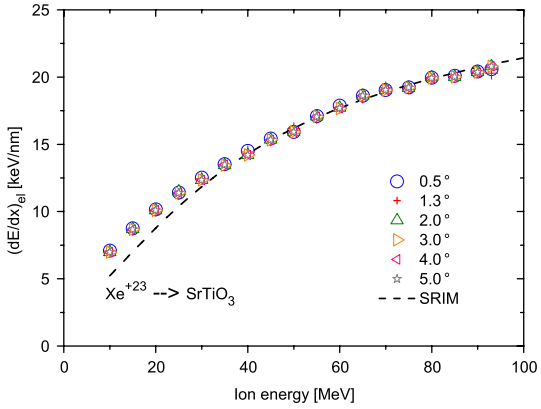

Figure 3. Stopping power as a function of ion energy for different polar angles of incidence. For each ion energy the stopping power has been averaged over the entire range of the azimuthal angle. The dashed line represents the calculated energy loss using SRIM [11].

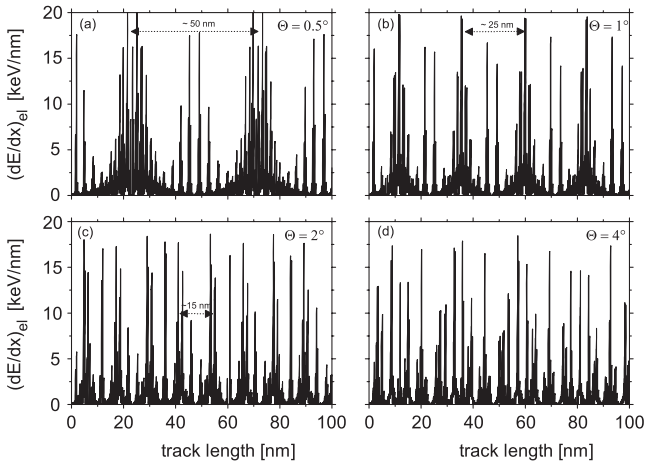

Figure 4. Electronic stopping power as a function of track length, i.e. travelled distance of the ion from the point of impact. Data has been calculated for a Xe^{23+} ion of 93 MeV initial kinetic energy penetrating a $SrTiO_3$ target under polar angles $\Theta = 0.5°$ (a), $\Theta = 1°$ (b), $\Theta = 2°$ (c) and $\Theta = 4°$ (d), respectively. The arrows represent the periodicity lengths of subsequent peaks of the same type as explained in detail in the text.

Figure 2 shows the dependence of the electronic stopping power, averaged along the trajectory, on the azimuthal angle of incidence for exemplary irradiation energies of 10, 50 and 90 MeV. The impact point of the projectile is located as illustrated in figure 1. The polar angle has been chosen as $\Theta = 0.5°$ with respect to the surface plane. Considering the stopping powers obtained we observe rather moderate fluctuations ($\sigma \approx 3\%$) around the mean values of 21.1 keV nm^{-1} (90 MeV), 15.3 keV nm^{-1} (50 MeV) and 6.7 keV nm^{-1} (10 MeV), respectively. The fine structures obtained in the angular dependence of the stopping power are directly related to the inhomogeneous electron density distribution and exhibit identical curve characteristics independent of the ion energy. The pronounced peaks at 19°, 27° and 34° correspond to low-indexed crystallographic directions for the chosen impact point. Minima in the electronic stopping close to the [001] direction are due to the presence of the Sr atom. The ratio of the amplitudes between the different projectile energies scales with $\sqrt{E}$ due to the Lindhard stopping cross section employed.

In order to verify the accuracy of our approach we calculate the stopping power averaged over the azimuthal degree of freedom for different ion energies and compare these values with SRIM calculations. The results are depicted in figure 3 for various polar angles of incidence Θ. It becomes directly obvious that the stopping power is largely independent of the angular degrees of freedom. In the energy range from (30–80) MeV the computed averaged stopping powers are in accordance with SRIM data. For impact energies below 30 MeV, however, we observe a systematic overestimation compared to the SRIM results. This deviation may be ascribed to different parameterizations of the energy dependence of the electronic stopping power in that energy regime.

Summarizing up to here, the averaged electronic stopping power appears to be independent of the particular choice of angular impact parameters and compares well with SRIM data. However, experiments clearly reveal the explicit dependence of the geometry of nano-surface dots (e.g. total chain length, periodicity length) on the particular choice of polar angle. Therefore, it is necessary to get an insight how the spatial characteristics of the energy transfer process along the ion track depends on the particular choice of the polar angle of incidence. It should be emphasized here, that this insight cannot in principle be obtained from SRIM calculations due to the fact that SRIM only uses effective electron densities averaged over an elementary unit cell. This is the reason why we instead employ *ab initio* data that provides the basis for studying the space-dependent energy deposition along the track and its correlation to the experimentally observed non-continuous surface modifications.

Figure 4 illustrates the calculated electronic stopping power along the 93 MeV Xe^{23+} ion track in $SrTiO_3$ for $\Theta = 0.5°$, $\Theta = 1°$, $\Theta = 2°$ and $\Theta = 4°$, respectively. For the purpose of clarity the depicted trajectory length is limited to 100 nm. The azimuthal angle is chosen as $\varphi = 7°$ representing a highly indexed direction. For $\Theta = 0.5°$ (see figure 4(a)) we notice two pronounced peaks at 20 and 70 nm track length. In the middle of those peaks we detect more thinned-out secondary peaks of approximately the same half

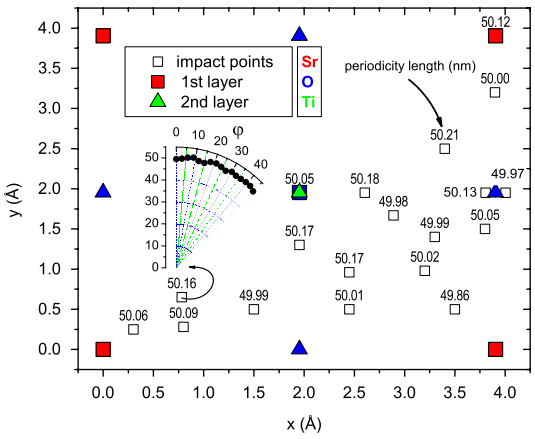

Figure 5. Top view onto one unit cell of the $SrTiO_3$ model crystal. Atoms are marked by full squares ('■') (first layer) or full triangles ('▲') (second layer) and coloured according to their elemental type (*red*: Sr; *green*: Ti; *blue*: O). In addition, the lateral distribution of impact points ('□') is illustrated. Each impact point is assigned a numerical value that constitutes the corresponding calculated periodicity length l_p (nm) averaged over the azimuthal angle φ as described in the main text. For one selected impact point located at position $x = 0.78$ Å and $y = 0.75$ Å a polar plot shows the periodicity lengths p_l obtained as a function of azimuthal angle of incidence with respect to the y-axis.

width contributing about 35% to the total excitation energy. Each of the peaks exhibits a fine structure of δ-shaped peaks naturally resulting from fluctuating electron densities along the track.

At this point we remark that a higher-resolved representation of the data would mirror the energy deposition during the passage of each unit cell. However, in our case the main point of interest is the observed distance between two consecutive areas of increased electronic stopping. The periodicity length derived for $\Theta = 0.5°$ is approximately 50 nm. For a slightly increased polar angle of 1° (see figure 4(b)) the same kind of peaks can be identified, however, each kind with a reduced periodicity of approximately 25 nm. For even larger polar angles of $\Theta = 2°$ and 4°, respectively, the two types of peaks begin to merge leading to a nearly constant enveloping function. Thus, the pronounced peak structure as seen before is increasingly smeared out and the periodicity tends to disappear.

In order to supply a qualitative explanation of the phenomenon that the periodic nanodot formation is limited to very glancing polar angles of incidence, the effect of the particular choice of impact point and azimuthal angle of incidence φ has to be investigated. Therefore, for each of the four selected polar angles, the calculation of the periodicity lengths has been carried out for 12 different impact points distributed within a triangular irreducible surface cell (see figure 5). Additionally, for each of these impact points, φ has been rasterized from 0° to 45° with respect to the y-axis using a step width of 3°. Note that it is sufficient to cover this angular interval due to crystallographic symmetry.

Representatively in view of statistical fluctuations, figure 5 depicts for $\Theta = 0.5°$ and for each impact point the calculated periodicity lengths l_p averaged over the different 15 azimuthal angles. It is obvious that the fluctuations of l_p are below 1% and, thus, completely negligible. Moreover, the statistical analysis reveals that l_p is also almost independent of φ. As an example, figure 5 contains a polar subplot of the φ-dependence of l_p for one arbitrarily selected impact point located at ($x = 0.78$ Å, $y = 0.75$ Å). Again, the relative deviations from the mean value of $l_p \approx 50$ nm are below 1%. This value of 50 nm is in good agreement with the experimentally observed peak separation (see [9], figure 6(a)).

Thus, the calculations presented here reveal the physical origin of the experimentally found polar-angle dependent threshold behaviour of periodic nanodot formation under glancing swift heavy ion irradiation of perovskites.

We are well aware that a more quantitative treatment of defect formation using our model must incorporate a realistic description of the transport of the excitation energy as well as the coupling of the electronic system to the lattice. This may be achieved in terms of a two temperature approach [19] as employed, for instance, in the thermal spike model [2]. However, in our case the anisotropy of the electron density and the necessity to properly implement the surface leads to a break-down of the radial symmetry usually presumed in standard thermal spike calculations and, thus, to a drastic increase in computational effort to numerically solve the corresponding transport equations. Calculations of this type are currently under way in our lab.

4. Conclusion

We have presented a model that uses highly-resolved *ab initio* electron density data in combination with molecular dynamics in order to obtain space-resolved electronic excitation characteristics along the track of swift heavy ions in matter. The model has been applied to the irradiation of $SrTiO_3$ with swift Xe^{23+} ions in a glancing incidence geometry for different ion energies and angular configurations of incidence.

Results for the average electronic stopping power are in good agreement with SRIM and, moreover, do not show a significant influence from a particular choice of the angular degree of freedom. However, the specific choice of the polar angle turns out to be crucial for the spatial distribution of electronic excitation along the ion track. A detailed analysis of the local behaviour of the electronic stopping power along the trajectory of the primary particle reveals a pronounced periodic structure that qualitatively explains the physical origin of periodic nanodot formation at insulator surfaces.

Finally, we would like to point out that our approach is applicable to any insulating material for which the electron density data can be calculated.

Acknowledgments

The authors would like to acknowledge financial support from the Deutsche Forschungsgemeinschaft within the Sonderforschungsbereiche 616 entitled *Energy Dissipation at Surfaces* and 445 entitled *Nano Particles from the Gas Phase*.

References

[1] Itoh N and Stoneham A M 2001 *Materials Modification by Electronic Excitation* (Cambridge: Cambridge University Press)

[2] Toulemonde M, Assmann W, Dufour C, Meftah A and Trautmann C 2006 Experimental phenomena and thermal spike model description of ion tracks in amorphisable inorganic insulators *Mat. Fys. Medd. Dan. Vid. Selsk.* **52** 263–92

[3] Weidinger A 2004 Ion tracks—a new route to nanotechnology *Europhys. News* **35**

[4] Khalfaoui N, Rotaru C C, Bouffard S, Toulemonde M, Stoquert J P, Haas F, Trautmann C, Jensen J and Dunlop A 2005 *Nucl. Instrum. Methods* B **240** 819–28

[5] Garcia-Navarro A, Mendez A, Olivares J, Garcia G, Agulla-Lopez F, Zayat M, Levy D and Vazquez L 2006 *Nucl. Instrum. Methods* B **249** 172–6

[6] Müller C, Benyagoub A, Lang M, Neumann R, Schwartz K, Toulemonde M and Trautmann C 2003 *Nucl. Instrum. Methods* B **209** 175–8

[7] Skuratov V A, Zinkle S J, Efimov A E and Havancsak K 2003 *Nucl. Instrum. Methods* B **203** 136–40

[8] Akcöltekin E, Peters T, Meyer R, Duvenbeck A, Klusmann M, Monnet I, Lebius H and Schleberger M 2007 Creation of multiple nanodots by single ions *Nat. Nanotechnol.* **2** 290–4

[9] Akcöltekin E, Akcöltekin S, Osmani O, Duvenbeck A, Lebius H and Schleberger M 2008 Swift heavy ion irradiation of $SrTiO_3$ under grazing incidence *New J. Phys.* **10** 053007

[10] Khalfaoui N, Görlich M, Müller C, Schleberger M and Lebius H 2006 *Nucl. Instrum. Methods* B **245** 246

[11] SRIM 2008 Software Package http://www.srim.org

[12] Biersack J P and Haggmark L G 1980 *Nucl. Instrum. Methods* B **174** 257

[13] Lindhard J and Scharff M 1961 Energy dissipation by ions in the keV region *Phys. Rev.* **124** 128

[14] Shima K, Ishihara T, Miyoshi T and Mikumo T 1983 Equilibrium charge-state distributions of 35–146 MeV Cu ions behind carbon foils *Phys. Rev.* A **28** 2162

[15] Shima K, Kuno N and Yamanouchi M 1989 Systematics of equilibrium charge distributions of ions passing through a carbon foil over the ranges $Z = 4$–92 and $E = 0.02$–6 MeV/u *Phys. Rev.* A **40** 3557

[16] Gonze X, Beuken J M, Caracas R, Detraux F, Fuchs M, Rignanese G M, Sindic L, Verstraete M, Zerah G, Jollet F, Torrent M, Roy A, Mikami M, Ghosez Ph, Raty J Y and Allan D C 2002 First-principles computation of material properties: the ABINIT software project *Comput. Mater. Sci.* **25** 478–92

[17] Fuchs M and Scheffler M 1999 *Comput. Phys. Commun.* **119** 67–98

[18] Perdew J P, Burke K and Ernzerhof M 1996 *Phys. Rev. Lett.* **77** 3865–8

[19] Anisimov S I, Bonch-Bruevich A M, Elyashevich M A, Imas Y A, Pavlenko N A and Romanov G S 1966 *Zh. Tekh. Fiz.* **36** 1273